ARTICLE

Application of dynamic mode decomposition to Rossi-α method in a critical state using file-by-file moving block bootstrap method

Tomohiro Endo[a*], Fuga Nishioka[a], Akio Yamamoto[a], Kenichi Watanabe[b], Cheol Ho Pyeon[c]

[a] *Department of Applied Energy, Graduate School of Engineering, Nagoya University, Furo-cho, Chikusa-ku, Nagoya, Aichi, 464-8603, Japan;*

[b] *Department of Applied Quantum Physics and Nuclear Engineering, Graduate School of Engineering, Kyushu University, 744 Motooka, Nishi-ku, Fukuoka, Fukuoka 819-0395, Japan;*

[c] *Institute for Integrated Radiation and Nuclear Science, Kyoto University, Asashiro-nishi, Kumatori-cho, Sennan-gun, Osaka 590-0494, Japan*

Abstract

Prompt neutron decay constant α in a critical state is useful information to validate the numerically predicted ratio of the point kinetics parameters $\beta_{\mathrm{eff}}/\ell$, where β_{eff} and ℓ are effective delayed neutron fraction and prompt neutron lifetime, respectively. To directly measure α in a target critical system, this study proposes the application of the dynamic mode decomposition (DMD) to the reactor noise analysis based on the Rossi-α method. The DMD-based Rossi-α method enables us to robustly estimate the fundamental mode component of α from the Rossi-α histograms measured using multiple neutron detectors. Furthermore, the file-by-file moving block bootstrap method is newly proposed for the statistical uncertainty quantification of α to prevent huge memory usage when the neutron count rate is high and/or the total measurement time is long. A critical experiment has been conducted at Kyoto University Critical Assembly to demonstrate the proposed method. As a result, the proposed method can uniquely determine the α value of which the statistical uncertainty is smallest. By utilizing this experimental result of α, numerical results of $\beta_{\mathrm{eff}}/\ell$ ratio using the continuous

*Corresponding author. Email: t-endo@energy.nagoya-u.ac.jp

energy Monte Carlo code MCNP6.2 with recent nuclear data libraries, which are processed by the nuclear data processing code FRENDY, are validated.

Keywords; prompt neutron decay constant; Rossi-α method; critical experiment; dynamic mode decomposition; bootstrap method; KUCA; validation; JENDL; FRENDY; MCNP

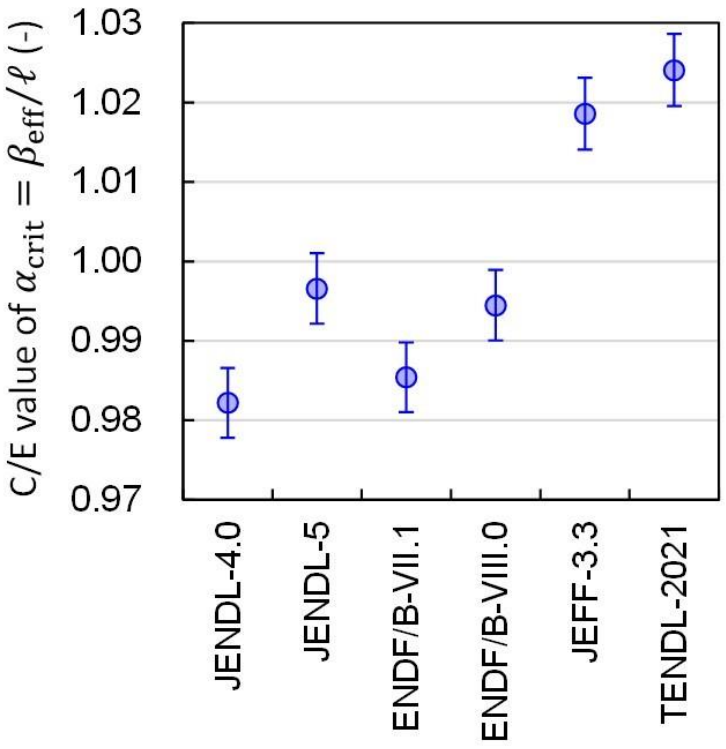

1. Introduction

In the field of reactor physics, the critical experiment has played an important role. To validate the criticality calculation using a neutron transport code with an evaluated nuclear data library, critical experimental results collected in databases such as the International Criticality Safety Benchmark Evaluation Project (ICSBEP) [1] are often utilized [2]. These critical experiments are also useful to estimate a calculational margin of effective neutron multiplication factor k_{eff} to judge the criticality for an application system [3,4]. Furthermore, the data assimilation using the critical experiments has the potential to update the evaluated nuclear data for better numerical prediction of k_{eff} [5].

Instead of k_{eff}, other neutronics parameters also attract attention for the validation and the data assimilation of the reactor physics calculation. For example, we have been investigating the usefulness of the prompt neutron decay constant α [6–10]. The physical meaning is the exponential decay of the fundamental mode for time variation in prompt neutron flux caused by a source neutron. The time constant α can be well approximated by $\alpha \approx (1-(1-\beta_{\mathrm{eff}})k_{\mathrm{eff}})/\ell$ in a near-critical state, where β_{eff} and ℓ are the effective delayed neutron fraction and the prompt neutron lifetime, respectively. In the critical state ($k_{\mathrm{eff}} = 1$), the α value (hereafter, denoted by α_{crit}) just corresponds to the ratio of $\beta_{\mathrm{eff}}/\ell$. As presented in a previous study [6], the nuclear data-induced correlations among β_{eff}, ℓ, and k_{eff} are small. Thus, the experimental result of α_{crit} is another useful information to independently validate the reactor physics calculation from other viewpoints related to the delayed neutron fraction of the main fissile nuclide and the neutron loss rate depending on the neutron energy spectrum in the measurement system.

As reported in previous studies [11–13], the α_{crit} value can be experimentally estimated from the experimental results of α in subcritical states. If subcriticality of a measurement system can be easily changed by the neutron absorber (e.g., control rod) and α values in the subcritical system can be measured by the reactor noise analysis method [14,15] or the pulsed

neutron source method [16], the α_{crit} value can be estimated by the extrapolation method for the variation in α with respect to k_{eff}. Note that the extrapolation method inevitably causes the extrapolation error of α_{crit} at $k_{\mathrm{eff}} = 1$. As another technique, if the subcriticality in the dollar units $-\rho/\beta_{\mathrm{eff}}$ can be measured by some kind of measurement techniques (e.g., the area ratio method [17]), the α_{crit} value can be estimated by correcting the measured α value in the subcritical state using the measured $-\rho/\beta_{\mathrm{eff}}$ value. Note that these experimental results of α and $-\rho/\beta_{\mathrm{eff}}$ depend on the neutron detector positions because the higher mode component affects the α-fitting and the area ratio methods [13]. Thus, a systematic error due to the higher mode component is another issue in estimating α_{crit}. Namely, some engineering judgement is required to uniquely determine the α value from multiple experimental results using multiple neutron detectors in different positions [8].

In this paper, we aim to address the issue in the measurement of α_{crit} by applying the dynamic mode decomposition (DMD) [18] to the reactor noise analysis using the Rossi-α method [19]. In addition, to clarify the usefulness of the measured $\beta_{\mathrm{eff}}/\ell$ value, we aim to validate numerical results of $\beta_{\mathrm{eff}}/\ell$ using the continuous energy Monte Carlo code MCNP6.2 [20,21] with different evaluated nuclear data libraries [22–26] that include recently released TENDL-2021 [27,28] and JENDL-5 [29,30]. Instead of using the extrapolation method, the Rossi-α method enables us to directly estimate α_{crit} from the reactor noise measurement in a delayed critical state [15]. Furthermore, the application of DMD to the Rossi-α histograms using the multiple neutron detectors enables us to robustly estimate the fundamental mode component of α_{crit}. To prevent the use of huge memories for the statistical uncertainty quantification of α_{crit}, we newly propose the file-by-file technique for the moving block bootstrap method [31–36] for reactor noise data, where the neutron count rate is high and/or the total measurement time is long.

The remainder of the paper is organized as follows. In Section 2, methodologies about the DMD-based Rossi-α and the file-by-file moving block bootstrap methods are explained.

Section 3 presents experimental analysis using the proposed method for a reactor noise measurement in a critical state, which was conducted at the Kyoto University Critical Assembly (KUCA) [37,38], followed by the validation for numerical results of $\beta_{\mathrm{eff}}/\ell$ using MCNP6.2. Concluding remarks are summarized in Section 4.

2. Methodology

2.1. Rossi-α method

The Rossi-α method [15] is a reactor noise analysis method to measure the prompt neutron decay constant α. For a target measurement system in a steady-state, let us consider that time-series data of neutron-detection-time (i.e., the reactor noise) is continuously measured from $t = 0$ to $t = T$, i.e., the total measurement time is T. Then, the neutron-detection-time interval τ is calculated for each combination of all neutron pairs detected within the range of $0 \leq t \leq (T - \tau_{\mathrm{UL}})$ to obtain the Rossi-α histogram $P(\tau)$ within the range of $0 \leq \tau \leq \tau_{\mathrm{UL}}$. Here, τ_{UL} is an upper limit of τ and determined by several times of $1/\alpha$.

Although more rigorous theoretical derivation for the analytical solution of the Rossi-α method in a critical state is a future research topic, let us assume that a target system in a delayed critical system with zero power can be regarded as an extremely shallow subcritical system driven by inherent neutron sources in nuclear fuels [39]. Based on the heuristic method using the Green's function that is expanded by the prompt α-eigenfunctions, the theoretical formula for $P(\tau)$ can be reasonably solved by utilizing the pair-detection probability [19,40]:

$$P(\tau) = \sum_{n=0}^{\infty} p_n \exp(-\alpha_n \tau) + C, \tag{1}$$

where α_n is the nth order prompt α-eigenvalue and α_0 corresponds to the fundamental mode component of the prompt neutron decay constant; p_n is the nth order expansion coefficient; and C means a constant component due to the uncorrelated term representing the frequency due to independent neutron pairs, which belong to different fission-chain families.

As shown in Equation (1), the histogram $P(\tau)$ has the exponential higher mode components and the constant component. If the higher mode components are sufficiently small, the fundamental mode component of $\alpha = \alpha_0$ can be estimated by fitting the following simple formula to the measured histogram $P(\tau)$:

$$P(\tau) = p_0 \exp(-\alpha\tau) + C. \quad (2)$$

In the conventional fitting method, Equation (2) is generally utilized to estimate α by excluding $P(\tau)$ data within a masking time interval ($0 \leq \tau \leq \tau_{\mathrm{mask}}$) to reduce the effect due to the higher mode components. Therefore, the estimated α value changes depending on the masking time τ_{mask}.

2.2. DMD-based Rossi-α method

To address the issue to extract the fundamental mode component from the measured Rossi-α histograms using multiple neutron detectors, we proposed the application of DMD [19]. In this section, the application procedure of the DMD-based Rossi-α method is briefly explained.

Let us prepare an $M \times N$ data matrix of Rossi-α histograms, where M is the total number of neutron detectors, N corresponds to the total number of time-bins for the histograms, and the bin width is $\Delta\tau$. Note that each of Rossi-α histograms is separately obtained without cross-counting for each of M detectors. Furthermore, to easily separate the constant component C in Equation (1) and to reduce the statistical uncertainty of α in the DMD analysis, a constant signal for all time-bins is virtually added to the data matrix. The effectiveness of adding the constant signal was experimentally demonstrated in the previous study [19].

As a result, the $(M+1) \times N$ data matrix $\mathbf{X} = \left(\vec{P}_1 \quad \vec{P}_2 \quad \cdots \quad \vec{P}_N\right)$ is prepared for the DMD analysis, where $\vec{P}_j$ represents the $(M+1)$-dimensional column vector at the jth time-bin and consists of $P(\tau)$ values measured by M detectors (from the first to the Mth element) and the constant signal ($(M+1)$th element). By taking the first or second through $(N-1)$th

or Nth column vectors, respectively, from the original matrix $\mathbf{X}$, two $(M+1)\times(N-1)$ slicing matrices $\mathbf{X}_{1:N-1}$ and $\mathbf{X}_{2:N}$ are obtained. Then, the relationship between $\mathbf{X}_{1:N-1}$ and $\mathbf{X}_{2:N}$ can be expressed using the following time evolution matrix $\mathbf{A}$:

$$\mathbf{A}\mathbf{X}_{1:N-1} = \mathbf{X}_{2:N}. \tag{3}$$

Equation (3) assumes that the time evolution of $\mathbf{X}_{2:N}$ at the next time-bin can be modeled by pre-multiplying $\mathbf{X}_{1:N-1}$ at the previous time-bin by the matrix $\mathbf{A}$. Based on Equation (3), the time evolution matrix $\mathbf{A}$ can be numerically evaluated using the data-driven approach. For this purpose, the singular value decomposition (SVD) is applied to $\mathbf{X}_{1:N-1}$:

$$\mathbf{X}_{1:N-1} = \mathbf{U}\mathbf{\Sigma}\mathbf{V}^{*}, \tag{4}$$

where $\mathbf{U}$ and $\mathbf{V}$ are unitary matrices consisting of left and right singular vectors; $\mathbf{\Sigma}$ is a diagonal matrix of which elements correspond to the singular values; the superscript $*$ means the conjugate transpose. Based on SVD shown in Equation (4), the pseudo-inverse matrix $\mathbf{X}_{1:N-1}^{+}$ can be analytically solved as follows:

$$\mathbf{X}_{1:N-1}^{+} = \mathbf{V}\mathbf{\Sigma}^{-1}\mathbf{U}^{*}, \tag{5}$$

where the superscript -1 means the inverse matrix. By multiplying Equation (3) by $\mathbf{X}_{1:N-1}^{+}$ from the right, the time evolution matrix $\mathbf{A}$ can be expressed as:

$$\mathbf{A} = \mathbf{X}_{2:N}\mathbf{V}\mathbf{\Sigma}^{-1}\mathbf{U}^{*}. \tag{6}$$

Then, the matrix $\mathbf{A}$ is projected onto $\mathbf{U}$ to obtain the DMD matrix $\widetilde{\mathbf{A}}$:

$$\widetilde{\mathbf{A}} = \mathbf{U}^{*}\mathbf{A}\mathbf{U} = \mathbf{U}^{*}\mathbf{X}_{2:N}\mathbf{V}\mathbf{\Sigma}^{-1}. \tag{7}$$

By applying the eigenvalue decomposition to $\widetilde{\mathbf{A}}$, the eigenvalues μ_i and eigenvectors $\vec{w}_i$ of $\widetilde{\mathbf{A}}$ are obtained for each mode ($1 \le i \le (M+1)$). Here, μ_i and $\vec{w}_i$ are sorted in the descending order of $\ln|\mu_i|/\Delta\tau$. After that, the eigenvectors $\vec{\phi}_i$ of $\mathbf{A}$ are reconstructed as follows:

$$\begin{gathered}\mathbf{\Phi} = \mathbf{X}_{2:N}\mathbf{V}\mathbf{\Sigma}^{-1}\mathbf{W}\,\mathrm{diag}(1/\mu_i), \\ \left(\begin{array}{c}\because \mathbf{A}\mathbf{\Phi} = \mathbf{\Phi}\mathrm{diag}(\mu_i), \widetilde{\mathbf{A}}\mathbf{W} = (\mathbf{U}^{*}\mathbf{A}\mathbf{U})\mathbf{W} = \mathbf{W}\mathrm{diag}(\mu_i), \\ \mathbf{A}\mathbf{U}\mathbf{W} = \mathbf{U}\mathbf{W}\mathrm{diag}(\mu_i), \mathbf{\Phi} = \mathbf{U}\mathbf{W}, \\ \mathbf{\Phi} = \mathbf{A}\mathbf{U}\mathbf{W}\mathrm{diag}(1/\mu_i) = (\mathbf{X}_{2:N}\mathbf{V}\mathbf{\Sigma}^{-1}\mathbf{U}^{*})\mathbf{U}\mathbf{W}\mathrm{diag}(1/\mu_i).\end{array}\right)\end{gathered} \tag{8}$$

where $\mathbf{\Phi} = (\vec{\phi}_1 \quad \vec{\phi}_2 \quad \cdots \quad \vec{\phi}_{M+1})$; $\mathbf{W} = (\vec{w}_1 \quad \vec{w}_2 \quad \cdots \quad \vec{w}_{M+1})$; and $\mathrm{diag}(x_i)$ represents the diagonal matrix where the (i,i)th element corresponds to x_i.

Consequently, the original data $\vec{P}_j$ can be expanding using the eigenvector matrix $\mathbf{\Phi}$:

$$\vec{P}_j = \sum_{i=1}^{M+1} c_i \vec{\phi}_i \exp(\omega_i (j-1)\Delta\tau), \tag{9}$$

where c_i and ω_i are expansion coefficient and time constant for the ith eigenvector $\vec{\phi}_i$. The expansion coefficients can be evaluated by multiplying the column vector $\vec{P}_1$ at the initial time-bin by the pseudo-inverse matrix $\mathbf{\Phi}^+$ from the left:

$$(c_1 \quad c_2 \quad \cdots \quad c_{M+1})^{\mathrm{T}} = \mathbf{\Phi}^+ \vec{P}_1, \tag{10}$$

where the superscript T means transpose. The time constant ω_i is evaluated from the eigenvalues μ_i of the time evolution matrix $\mathbf{A}$:

$$\omega_i = \frac{\ln(\mu_i)}{\Delta\tau}. \tag{11}$$

Based on the eigenvector expansion results shown in Equations (9)–(11), the DMD-based Rossi-α method can extract the fundamental mode component of α. Because the time constant for the constant component in Equation (9) corresponds to zero ($\omega_1 = 0$), the fundamental mode component of α can be finally evaluated by the second maximum eigenvalue μ_2:

$$\alpha = -\omega_2 = -\frac{\ln(\mu_2)}{\Delta\tau}. \tag{12}$$

Note that the prompt neutron decay constant is a negative time constant and that the sign of α is opposite to that of ω_2.

2.3. File-by-file moving block bootstrap method

When the reactor noise analysis is applied to measure α in a critical state, there are the following issues to quantify the statistical uncertainty of α using the Rossi-α method. First, the Rossi-α histogram has strong correlations between different neutron-detection-time

intervals τ because $P(\tau)$ is generally estimated by reusing the same reactor noise data. These strong correlations complicate the statistical uncertainty quantification of α. The first issue can be addressed using the moving block bootstrap method [33] to take the correlations into account as presented in previous studies [35,36]. Second, since the neutron count rate in the critical state is higher than that in a subcritical state, the moving block bootstrap method requires more memories as the total measurement time becomes longer to reduce the statistical uncertainty. To address the second issue, we newly propose the file-by-file moving block bootstrap method.

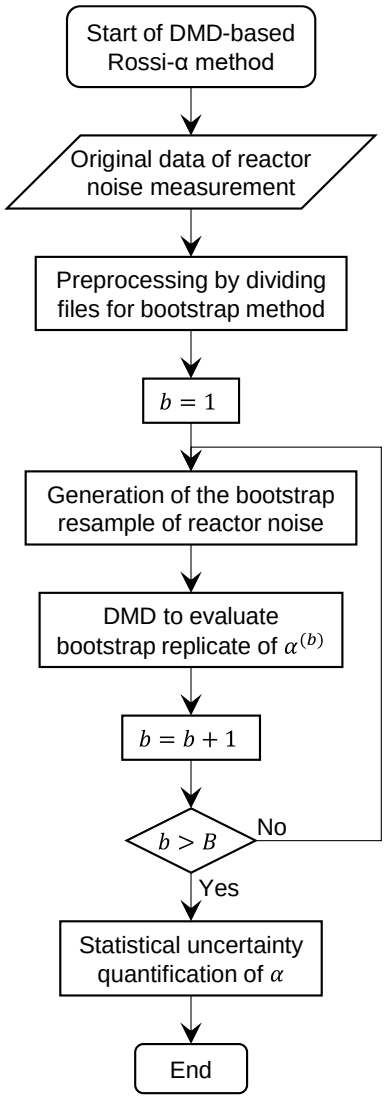

Figure 1 Flowchart of file-by-file moving block bootstrap method

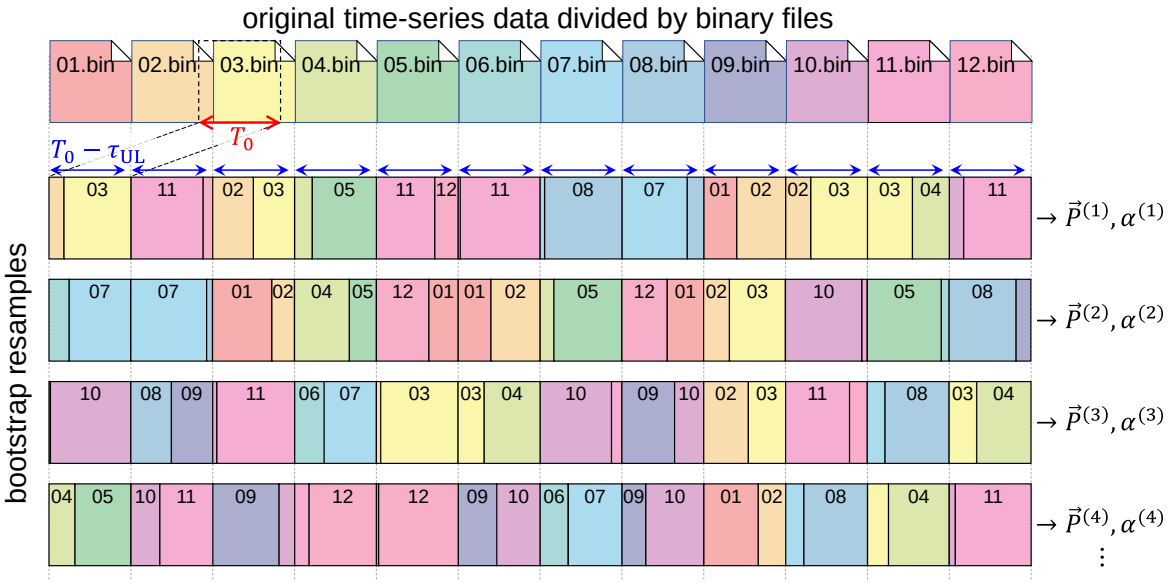

Figure 2 Example of file-by-file moving block bootstrap method ($F = 12$)

To promote better understanding of the proposed method, **Figure 1** and **Figure 2** show a flowchart and a simple example of the proposed method, respectively. The detailed procedures are explained below:

1. Original list mode data, which consist of pairs of neutron-detection-time and detector-channel-number, are provided by a single measurement of reactor noise.
2. The original data are divided by successive binary files per a fixed time interval T_0 (e.g., $T_0 = 5$ s). The total number of binary files is F, i.e., the total measurement time of the original reactor noise corresponds to FT_0. Here, the file name is indexed as 'xxx.bin' where the file-identifier xxx is a zero-filled integer (e.g., $001 \leq \text{xxx} \leq 900$ when $F = 900$). In this study, the time interval T_0 is set to handle each binary file using smaller memories, on the condition that $T_0 \gg \tau_{UL}$ and F is larger than several hundred.
3. The bootstrap resampling procedure is started ($b = 1$), where the index b represents the bth bootstrap resampling calculation.
4. For resampling arbitrary time-series data within a range of $t' \leq t \leq (t' + T_0)$ from the successively divided binary files, resampling index ξ_{xxx} for the file-identifier xxx is firstly

determined using a uniform random integer number, $1 \leq \xi_{\mathrm{xxx}} \leq F$. Then, the next file-identifier yyy is determined by the zero-filled integer of $(\xi_{\mathrm{xxx}} + 1)$. Note that yyy is 001 if $\xi_{\mathrm{xxx}} = F$ because the periodic condition for the time-series data is assumed in the present study. Towards the slicing process in step 5, the two successive binary files 'xxx.bin' and 'yyy.bin' are resampled and read to temporarily store the $2T_0$ data on memories.

5. From the stored data where the time range is $0 \leq t \leq 2T_0$, the time-series data within the range of $\xi_T \leq t \leq (\xi_T + T_0)$ is sliced using a uniform random number $0 \leq \xi_T \leq T_0$. Then, as explained in Section 2.1, neutron-detection-time intervals τ are calculated for all neutron pairs within the range of $\xi_T \leq t \leq (\xi_T + T_0 - \tau_{\mathrm{UL}})$ to accumulate the Rossi-α histograms $\vec{P}^{(b)}$ with a constant bin width $\Delta\tau$ for each of M neutron detectors. Here, the superscript (b) indicates the bth bootstrap procedure.
6. Steps 4 and 5 are repeated F times to obtain the bth bootstrap replicate of $\mathbf{X}^{(b)}$ for DMD. Namely, the bootstrap sample of list mode data, of which total measurement time is $F(T_0 - \tau_{\mathrm{UL}})$, are virtually generated to carry out the DMD procedure.
7. Based on the DMD procedure explained in Section 2.2, the bth bootstrap replicate of prompt neutron decay constant $\alpha^{(b)}$ is evaluated using Equation (12).
8. To estimate the confidence intervals of $\vec{P}^{(b)}$ and $\alpha^{(b)}$, steps 4–7 are repeated B times. Consequently, bootstrap distributions for $\vec{P}^{(b)}$ and $\alpha^{(b)}$ are obtained ($1 \leq b \leq B$), where the total number of bootstrap replicates B is typically set as $B = 1000$ [32].
9. Based on these bootstrap distributions, statistical uncertainties of $\vec{P}^{(b)}$ and $\alpha^{(b)}$ can be easily estimated as follows. For example, the bootstrap standard deviations can be estimated by the square root of the unbiased variances for $\vec{P}^{(b)}$ and $\alpha^{(b)}$. Or, to evaluate the range of the statistical uncertainties of $\vec{P}^{(b)}$ and $\alpha^{(b)}$, the bootstrap confidence intervals can be simply estimated by the 2.5 and 97.5 percentile points. Let us sort the *B* bootstrap replicates $\alpha^{(b)}$ in ascending order. From the $(0.025 \times B)$th and $(0.975 \times B)$th smallest values of

sorted $\alpha^{(b)}$, the lower and upper limits of 95% bootstrap confidence interval are simply estimated, respectively.

3. Experimental Analysis

3.1. Experimental settings

To demonstrate the DMD-based Rossi-α method, a reactor noise experiment in a critical state was conducted in the A-core (A1/8"p60EUEU(3)+1/8"Pb40p20EUEU) at the KUCA [37,38]. The experimental and calculation conditions are briefly explained below.

The experimental cores and the loaded fuel assemblies are shown in **Figure 3** and **Figure 4**, respectively. In this experiment, four types of fuel assemblies were used [38]. Normal fuel assembly ('F' element: 1/8"p60EUEU) has 60 unit fuel-cells. The unit fuel-cell consists of two highly enriched uranium-aluminum alloy (HEU) plates 1/8" thick and one polyethylene plate 1/8" thick. Two partial fuel assemblies ('40' element: 1/8"p40EUEU; and '14' element: 1/8"p14EUEU) use the same unit fuel-cell as the normal fuel, although the total numbers of unit fuel-cells are 40 and 14, respectively, to adjust the excess reactivity. Test fuel assembly ('Pb' element: 1/8"Pb40p20EUEU) has 40 special unit cells, sandwiched between 10 normal unit cells on the top and 10 normal unit cells at the bottom. The special unit cell consists of two HEU plates 1/8" thick and one lead plate 1/8" thick instead of the polyethylene plate.

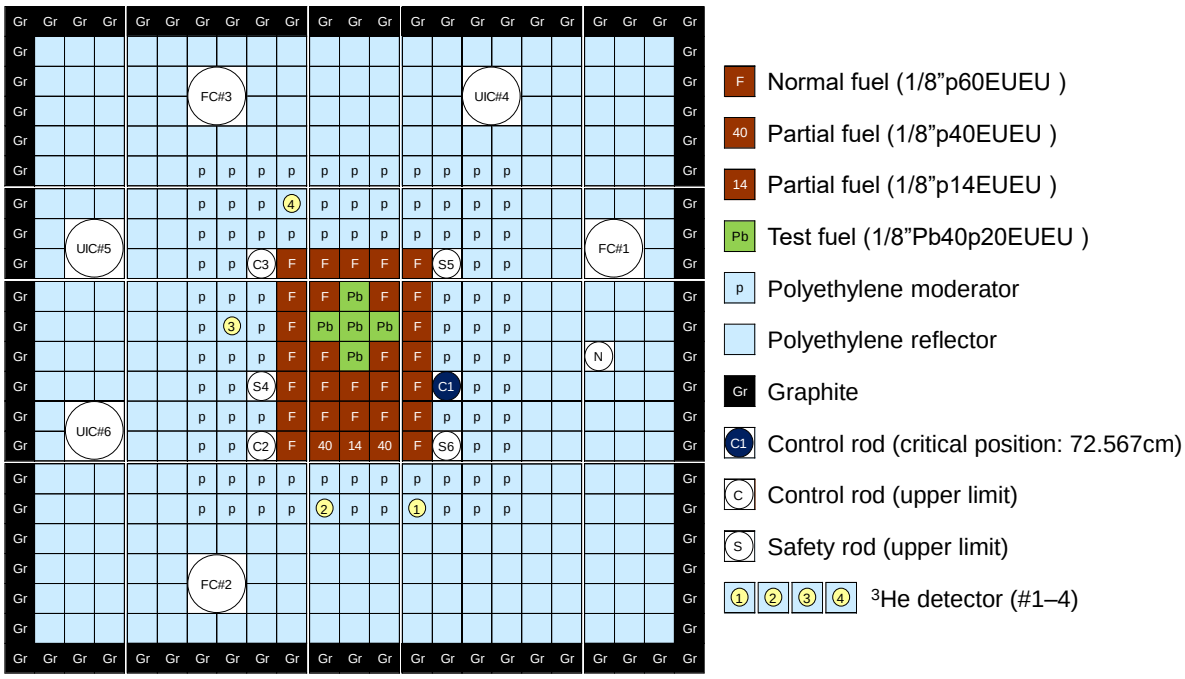

Figure 3 Top view of experimental core (A1/8”p60EUEU(3)+1/8”Pb40p20EUEU)

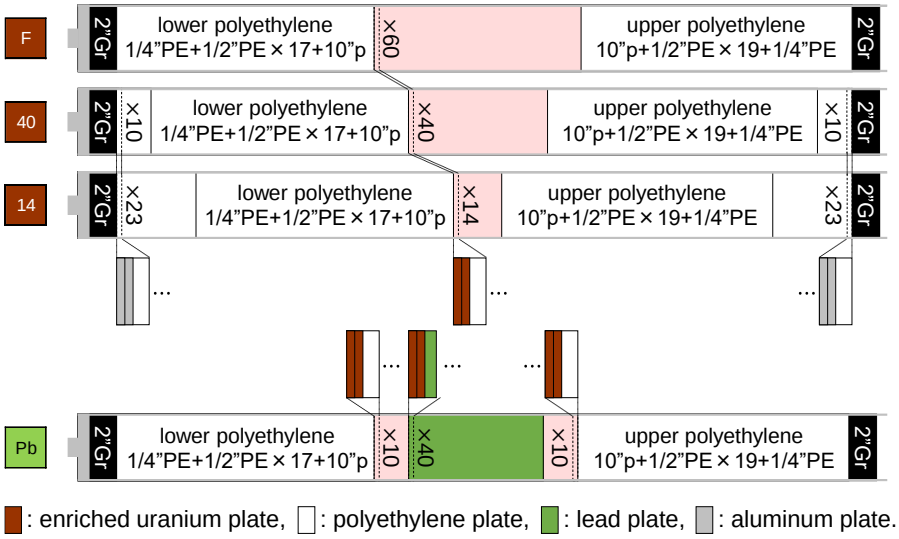

Figure 4 Side views of fuel assemblies

In this experiment, four ^{3}He detectors (#1–4) were placed at axially center positions of excore reflector assemblies, which have holes of approximately 3 cm in diameter to insert detectors. A digital MCA (ANSeeN, HSDMCA) was utilized to successively measure list mode data of neutron-detection-time and detector-channel-number. The experimental core was

maintained at a critical state by adjusting the C1 control rod position at 72.567 cm. In the critical state, average neutron count rates for ^{3}He#1–4 were 26377 ± 26, 29152 ± 27, 36212 ± 29, and 22383 ± 23 cps, respectively. To check whether a criticality bias due to the inherent neutron source in the HEU plate is negligibly small, the potential bias was roughly estimated based on the neutron source multiplication method [39]. In the deep subcritical core at the shutdown state ($k_{\text{eff}} = 0.91969 \pm 0.00003$ obtained by MCNP6.2 [20,21] with ENDF/B-VIII.0 [25]) without any external neutron source, magnitudes of neutron count rates for ^{3}He#1–4 were 10.62 ± 0.02, 12.27 ± 0.02, 13.99 ± 0.02, and 7.66 ± 0.01 cps, respectively. If the critical core in this experiment is regarded as a very shallow subcritical system driven by the inherent neutron source, the subcriticality is roughly estimated as $-\rho \approx \frac{12.27}{29152}\left(\frac{1}{0.92} - 1\right) \approx 4 \times 10^{-5} = 4$ pcm based on the neutron source multiplication factor method for the neutron count rates by ^{3}He#4. Then, the contribution of the potential bias due to the inherent neutron source on α_{crit} was $\frac{\alpha - \alpha_{\text{crit}}}{\alpha_{\text{crit}}} \approx \frac{(\beta_{\text{eff}} - \rho)/\Lambda - \beta_{\text{eff}}/\ell}{\beta_{\text{eff}}/\ell} \approx \frac{-\rho}{\beta_{\text{eff}}} \approx 0.5\%$, because $\Lambda \approx \ell$ and $\beta_{\text{eff}} \approx 800$ pcm as shown later in Equation (13) and **Table 1**. Thus, we judged that the inherent neutron source effect was negligible in this reactor noise experiment.

The total measurement time of the reactor noise at the critical state was $FT_0 = 4500$ s. In this experimental analysis, the parameters for the DMD-based Rossi-α and the file-by-file moving block bootstrap methods were set as follows: the time interval for each binary file $T_0 = 5$ s; the total number of binary files $F = 900$; the bin width of Rossi-α histogram $\Delta\tau = 0.0001$ s; the upper limit of τ for the Rossi-α histogram $\tau_{\text{UL}} = 0.02$ s; and the total number of bootstrap replicates $B = 1000$. For comparison, the α values for ^{3}He#1–4 were also estimated using the conventional fitting method for $P(\tau)$, where 'scipy.optimize.curve_fit' was utilized using the estimated uncertainties with the option of 'absolute_sigma=False' [41].

3.2. Experimental results

For each of neutron detectors, **Figure 5** shows the variations in the Rossi-α histograms with respect to the detection-time-interval τ. Since the total measurement time $FT_0 = 4500$ s is long, statistical uncertainties of Rossi-α histograms are very small, i.e., the magnitudes of relative standard deviations are approximately 0.07%.

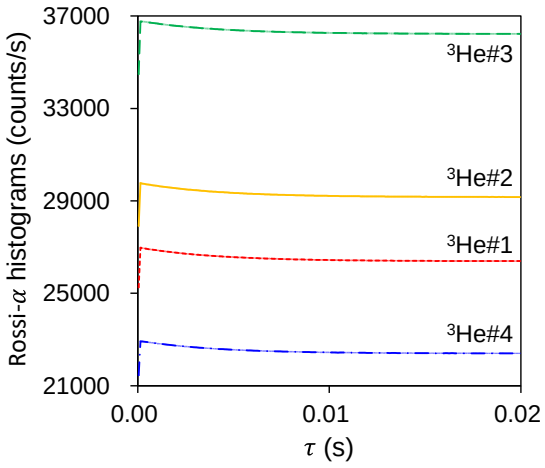

Figure 5 Rossi-α histograms

Next, **Figure 6** presents the variations in the prompt neutron decay constant α with respect to the masking time τ_{mask} using the conventional fitting method for each detector and using the DMD-based Rossi-α method, respectively. Here, the error bars indicate the 1.96σ of fitting errors for the conventional fitting method and the 95% bootstrap confidence intervals for the DMD-based Rossi-α methods, respectively. In both methods, estimated α values change according to the masking time τ_{mask}. As τ_{mask} becomes larger, the exponential decrease of fundamental component results in larger statistical uncertainty of the estimated α value. Interestingly noted that the estimated α values by the conventional fitting method slightly depend on the position of the neutron detector compared with the magnitude of fitting errors, although the detector-dependency in α is very small due to the less excitation of higher mode components in the critical state. For example, when the fitting errors are smallest, the estimated

α values are 244.7 ± 0.3, 245.7 ± 0.3, 248.3 ± 0.3, and 246.7 ± 0.3 (1/s), respectively. Thus, if a reference value of α for the target system is not available in advance, the conventional fitting method requires the engineering judgement to uniquely determine the α value, e.g., the selection of an appropriate detector position or the weighted average for the detector-dependent α values [8]. On the other hand, without the engineering judgement, the DMD-based Rossi-α method can uniquely evaluate α by extracting the fundamental mode component from all data using four neutron detectors. In this experimental analysis, the α_{crit} value is finally estimated as 245.1 ± 0.9 (1/s) when the statistical uncertainty by the file-by-file moving block bootstrap method is the smallest (gray-filled circle in **Figure 6-b**).

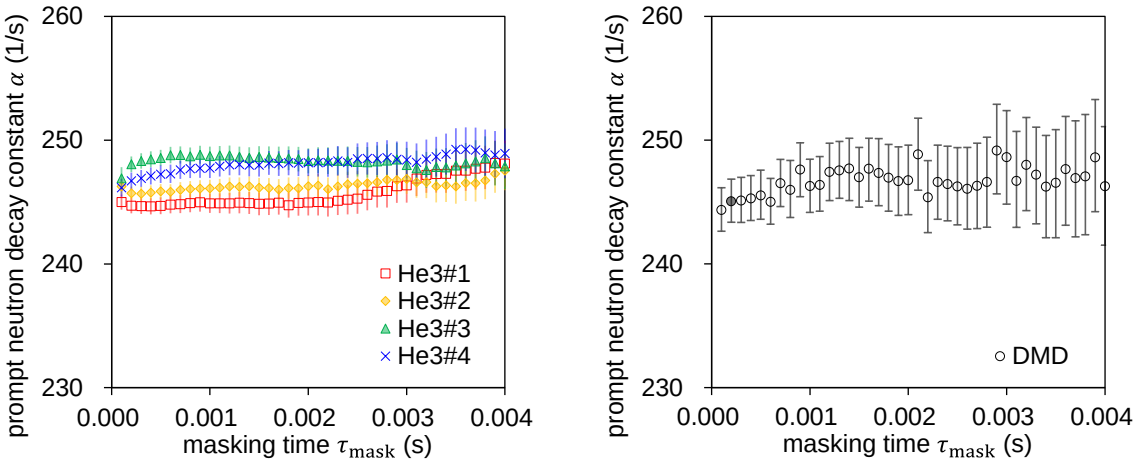

a) Conventional fitting method b) DMD-based Rossi-α method

Figure 6 Variation in α with respect to masking time

3.3. Validation for numerical results of $\beta_{\mathrm{eff}}/\ell$

To validate numerical results of $\beta_{\mathrm{eff}}/\ell$ using a continuous energy Monte Carlo calculation with evaluated nuclear data libraries, MCNP6.2 [20,21] calculations were carried out for JENDL-4.0 [22,23], JENDL-5 [29,30], ENDF/B-VII.1 [24], ENDF/B-VIII.0 [25], JEFF-3.3 [26], and TENDL-2021 [27,28]. Note that thermal scattering law data of ENDF-B/VIII.0 for H in CH_2, graphite with 30% porosity, and ^{27}Al were used in the calculation using TENDL-2021

because these data were not available in TENDL-2021 [28]. These ACE-formatted files were generated using the Japanese nuclear data processing code FRENDY (ver. 1.04.036) with 'weight_option=2 (tabulated)' for the thermal ACE files [42]. In the numerical analysis for the critical KUCA core, the nuclide composition and size for each material were quoted from Reference [37]. The total number of neutron histories was 1 billion, i.e., the neutron histories per cycle = 500000, active cycle = 2000, and inactive cycle = 100. The effective delayed neutron fraction β_{eff} and the neutron generation time Λ were evaluated based on the iterated fission probability method with the option of 'BLOCKSIZE = 5' in the KOPT card [43]. The prompt neutron lifetime ℓ was evaluated based on the following relationship [6]:

$$\ell = k_{\mathrm{eff}}\Lambda. \tag{13}$$

Table 1 summarizes the numerical results of k_{eff} and $\alpha_{\mathrm{crit}} = \beta_{\mathrm{eff}}/\ell$ using MCNP6.2 with JENDL-4.0, JENDL-5, ENDF/B-VII.1, ENDF/B-VIII.0, JEFF-3.3, and TENDL-2021, respectively. To validate these numerical results, C/E values of α_{crit} are also estimated using the experimental result of 245.1 ± 0.9 (1/s) by the DMD-based Rossi-α method. Consequently, the C/E values of α_{crit} exist within the range of 0.982–1.024, i.e., numerical results of $\beta_{\mathrm{eff}}/\ell$ by MCNP6.2 with FRENDY-processed ACE files agree well with the measured α_{crit}. Among recently available nuclear data libraries, this KUCA critical experiment supports the update (e.g., thermal scattering law data for H in CH_2) in ENDF/B-VIII.0 and JENDL-5 to accurately predict $\beta_{\mathrm{eff}}/\ell$ because the C/E value is 0.994 ± 0.004 and 0.997 ± 0.004, respectively. To clarify this reason, sensitivity analysis of $\beta_{\mathrm{eff}}/\ell$ with respect to nuclear data is necessary. However, this sensitivity analysis is an open problem in this study because MCNP6.2 cannot analyze the sensitivity of $\beta_{\mathrm{eff}}/\ell$. Thus, further sensitivity analysis of point kinetics parameters β_{eff} and ℓ for this experimental result is a future issue. This sensitivity analysis requires a complicated numerical analysis method based on the generalized perturbation theory. For example, the collision history-based approach in Serpent

2 [44] will enable us to accomplish this sensitivity analysis using the continuous energy Monte Carlo code.

Table 1 Numerical results of $\boldsymbol{\alpha_{\mathrm{crit}}}$

Nuclear data	k_{eff} (-)	β_{eff} (pcm)	Λ (s)	ℓ (s)	$\beta_{\mathrm{eff}}/\ell$ (s)	C/E of α_{crit} (-)
JENDL-4.0	0.99813±0.00003	802±2	33.377±0.014	33.314±0.014	240.7±0.6	0.982±0.004
JENDL-5	0.99677±0.00003	801±2	32.899±0.013	32.793±0.013	244.3±0.6	0.997±0.004
ENDF/B-VII.1	1.00083±0.00003	801±2	33.137±0.013	33.164±0.013	241.5±0.6	0.985±0.004
ENDF/B-VIII.0	0.99845±0.00003	797±2	32.749±0.013	32.698±0.013	243.7±0.6	0.994±0.004
JEFF-3.3	1.00153±0.00003	817±2	32.675±0.013	32.725±0.013	249.7±0.6	1.019±0.005
TENDL-2021	1.00073±0.00003	818±2	32.566±0.013	32.590±0.013	251.0±0.6	1.024±0.005

4. Conclusion

To directly and robustly estimate the fundamental mode component of α_{crit}, this study proposed the application of the DMD-based Rossi-α method to a reactor noise measurement in a critical state. Furthermore, to reduce the memory usage in the statistical uncertainty quantification of α_{crit} when the neutron count rate is high and/or the total measurement time is long, the file-by-file moving block bootstrap method was newly proposed. Through the critical experiment conducted at KUCA, the estimated α values by the conventional fitting method had a slight dependency on neutron detector position, which requires the engineering judgement such as the selection of an appropriate detector position or the weighted average for the detector-dependent α values. In contrast, it was demonstrated that the DMD-based Rossi-α method can uniquely determine the α_{crit} value of which the statistical uncertainty is smallest. Specifically, the α_{crit} value in this critical experiment was finally estimated as 245.1 ± 0.9 (1/s). By confirming that numerical results of point kinetics parameter ratio $\beta_{\mathrm{eff}}/\ell$ agreed well with this experimental result, we validated the MCNP6.2 calculations with

recent nuclear data libraries, which were processed by the recent Japanese nuclear data processing code FRENDY. Consequently, this study clarified the usefulness of measured α_{crit} to validate the reactor physics calculation from the viewpoint of $\beta_{\mathrm{eff}}/\ell$. To further discuss the impact of nuclear data on $\beta_{\mathrm{eff}}/\ell$, sensitivity analysis of β_{eff} and ℓ with respect to nuclear data is necessary as a future study.

Acknowledgments

This work has been carried out in part under the Visiting Researcher's Program of the Kyoto University. The authors are grateful to all the technical staff of KUCA for their assistance during the experiment. The authors would like to express our gratitude to Dr. Kenichi Tada for his continuous efforts in the improvement of FRENDY.

Funding

This work was supported by the Japan Society for the Promotion of Science (JSPS) Grant-in-Aid for Scientific Research (C) (Grant Number 19K05328).

References

1. Bess JD, Ivanova T, editors. International handbook of evaluated criticality safety benchmark experiments. Paris (France): OECD NEA; 2020. NEA/NSC/DOC(95)/03.
2. Chiba G, Okumura K, Sugino K, et al. JENDL-4.0 benchmarking for fission reactor applications. J Nucl Sci Technol. 2011;48(2):172–187.
3. Kiedrowski BC, Brown FB, Conlin JL, et al. Whisper: sensitivity/uncertainty-based computational methods and software for determining baseline upper subcritical limits. Nucl Sci Eng. 2015;181(1):17–47.
4. Hayashi T, Endo T, Yamamoto A. Proposal and applicability of estimated criticality lower-limit multiplication factor using the bootstrap method. J Nucl Sci Technol.

2021;58(9):1008–1017.

5. Rochman D, Bauge E, Vasiliev A, et al. Monte Carlo nuclear data adjustment via integral information. Eur Phys J Plus. 2018;133:537.
6. Endo T, Chiba G, van Rooijen WFG, et al. Experimental analysis and uncertainty quantification using random sampling technique for ADS experiments at KUCA. J Nucl Sci Technol. 2018;55(4):450–459.
7. Endo T, Yamamoto A. Sensitivity analysis of prompt neutron decay constant using perturbation theory. J Nucl Sci Technol. 2018;55(11):1245–1254.
8. Endo T, Watanabe K, Chiba G, et al. Nuclear data-induced uncertainty quantification of prompt neutron decay constant based on perturbation theory for ADS experiments at KUCA. J Nucl Sci Technol. 2020;57(2):196–204.
9. Endo T, Yamamoto A. Data assimilation using subcritical measurement of prompt neutron decay constant. Nucl Sci Eng. 2020;194(11):1089–1104.
10. Endo T, Noguchi A, Yamamoto A, et al. Perturbation-theory-based sensitivity analysis of prompt neutron decay constant for water-only system. Tran Am Nucl Soc. 2021;124(1):184–187.
11. Sakon A, Nakajima K, Hohara S, et al. Experimental study of neutron counting in a zero-power reactor driven by a neutron source inherent in highly enriched uranium fuels. J Nucl Sci Technol. 2019;56(2):254–259.
12. Yamanaka M, Pyeon CH, Endo T, et al. Experimental analyses of $\beta_{\mathrm{eff}}/\Lambda$ in accelerator-driven system at Kyoto University Critical Assembly. J Nucl Sci Technol. 2020;57(2):205–215.
13. Pyeon CH, Yamanaka M, Endo T, et al. Neutron generation time in highly-enriched uranium core at Kyoto University Critical Assembly. Nucl Sci Eng. 2020;194(12):1116–1127.
14. Feynman RP, de Hoffmann F, Serber R. Dispersion of the neutron emission in U-235 fission.

J Nucl Energy. 1956;3(1–2):64–69.

15. Orndoff JD. Prompt neutron periods of metal critical assemblies. Nucl Sci Eng. 1957;2(4):450–460.
16. Simmons BE, King JS. A pulsed neutron technique for reactivity determination. Nucl Sci Eng. 1958;3(5):595–608.
17. Sjöstrand NG. Measurements on a subcritical reactor using a pulsed neutron source. Arkiv för Fysik. 1956;11:233–246.
18. Schmid PJ. Dynamic mode decomposition of numerical and experimental data. J Fluid Mech. 2010;656:5–28.
19. Nishioka F, Endo T, Yamamoto A, et al. Applicability of dynamic mode decomposition to estimate fundamental mode component of prompt neutron decay constant from experimental data. Nucl Sci Eng. 2022;196(2):133–143.
20. Goorley T, James M, Booth T, et al. Features of MCNP6. Ann Nucl Energy. 2016;87(2):772–783.
21. Werner CJ, editor. MCNP user's manual code version 6.2. Los Alamos (NM): Los Alamos National Laboratory; 2017. LA-UR-17-29981.
22. Shibata K, Iwamoto O, Nakagawa T, et al. JENDL-4.0: a new library for nuclear science and engineering. J Nucl Sci Technol. 2011;48(1):1–30.
23. JENDL-4.0u and JENDL-4.0+ [Internet]. Ibaraki (Japan): Japan Atomic Energy Agency; [updated 2016 Jan 27; cited 2022 Jan 4]. Available from: https://wwwndc.jaea.go.jp/jendl/j40/update/
24. Chadwick MB, Herman M, Obložinský P, et al. ENDF/B-VII.1 nuclear data for science and technology: cross sections, covariances, fission product yields and decay data. Nucl Data Sheets. 2011;112(12):2887–2996.
25. Brown DA, Chadwick MB, Capote R, et al. ENDF/B-VIII.0: the 8th major release of the nuclear reaction data library with CIELO-project cross sections, new standards and thermal

scattering data. Nucl Data Sheets. 2018;148:1–142.
26. Plompen AJM, Cabellos O, de Saint Jean C, et al. The joint evaluated fission and fusion nuclear data library, JEFF-3.3. Eur Phys J A. 2020;56:181.
27. Koning AJ, Rochman D, Sublet J-Ch, et al. TENDL: complete nuclear data library for innovative nuclear science and technology. Nucl Data Sheets. 2019;155:1–55.
28. TENDL-2021 [Internet]. Villigen (Switzerland): Paul Scherrer Institut; [updated 2021 Dec 30; cited 2022 Jan 4]. Available from: https://tendl.web.psi.ch/tendl_2021/tendl2021.html
29. Iwamoto O, Iwamoto N, Shibata K, et al. Status of JENDL. EPJ Web Conf. 2020;239:09002.
30. JENDL-5 [Internet]. Ibaraki (Japan): Japan Atomic Energy Agency; [updated 2021 Dec 27; cited 2022 Jan 4]. Available from: https://wwwndc.jaea.go.jp/jendl/j5/j5.html
31. Efron B. Bootstrap methods: another look at the Jackknife. Ann Stat. 1979;7(1):1–26.
32. Efron B, Tibshirani RJ. An introduction to the bootstrap. New York (NY): Chapman & Hall; 1994.
33. Künsch HR. The Jackknife and the bootstrap for general stationary observations. Ann Stat. 1989;17(3):1217–1241.
34. Endo T, Yamamoto A, Yagi T, et al. Statistical error estimation of the Feynman-α method using the bootstrap method. J Nucl Sci Technol. 2016;53(9):1447–1453.
35. Endo T, Yamamoto A, Yamanaka M, et al. Experimental validation of unique combination numbers for third- and fourth-order neutron correlation factors of zero-power reactor noise. J Nucl Sci Technol. 2019;56(4):322–336.
36. Endo T, Yamamoto A. Comparison of theoretical formulae and bootstrap method for statistical error estimation of Feynman-α method. Ann Nucl Energy. 2019;124:606–615.
37. Pyeon CH, editor. Accelerator-driven system at Kyoto University Critical Assembly. Singapore: Springer Singapore; 2021.
38. Pyeon CH, Yamanaka M, Fukushima M. Uncertainty quantification of lead and bismuth

sample reactivity worth at Kyoto University Critical Assembly. Nucl Sci Eng. 2021;195(8):877–889.

39. Shiozawa T, Endo T, Yamamoto A, et al. Investigation on subcriticality measurement using inherent neutron source in nuclear fuel. Proceedings of the International Conference on Physics of Reactors (PHYSOR 2014); 2014 Sep 28–Oct 3; Kyoto, Japan. Ibaraki (Japan): Japan Atomic Energy Agency; 2015. (JAEA-Conf 2014-003).
40. Endo T, Yamane Y, Yamamoto A. Space and energy dependent theoretical formula for the third order neutron correlation technique. Ann Nucl Energy. 2006;33:521–537.
41. SciPy reference guide, release 1.7.1 [Internet]. SciPy.org; [updated 2021 Aug 1; cited 2022 Jan 4]. Available from: https://docs.scipy.org/doc/scipy/scipy-ref-1.7.1.pdf#page=1299
42. Tada K, Nagaya Y, Kunieda S, et al. Development and verification of a new nuclear data processing system FRENDY. J Nucl Sci Technol. 2017;54(7):806–817.
43. Kiedrowski BC, Brown FB, Wilson PPH. Adjoint-weighted tallies for *k*-eigenvalue calculations with continuous-energy Monte Carlo. Nucl Sci Eng. 2011;168(3):226–241.
44. Aufiero M, Bidaud A, Hursin M, et al. A collision history-based approach to sensitivity/perturbation calculations in the continuous energy Monte Carlo code SERPENT. Ann Nucl Energy. 2015;85:245–258